SUPPORTING INFORMATION

Linear Eyring Plots Conceal a Change in Rate-Limiting Step in an Enzyme Reaction

Teresa F. G. Machado,[†] Tracey M. Gloster,[‡] and Rafael G. da Silva*[,‡]

[†]School of Chemistry and [‡]School of Biology, Biomedical Sciences Research Complex, University of St Andrews, St Andrews, KY16 9ST United Kingdom.

*To whom correspondence may be addressed: rgds@st-andrews.ac.uk

MATERIALS AND METHODS

Materials. All commercially available chemicals were used without further purification. Reduced nicotinamide adenine dinucleotide (NADH), oxidised nicotinamide adenine dinucleotide (NAD^+), acetoacetate, imidazole, glycerol, lysozyme, DNase I, ampicillin, and kanamycin were purchased from Sigma-Aldrich. Ethylenediaminetetraacetic acid (EDTA)-free Cømplete protease inhibitor cocktail was purchased from Roche. Isopropyl *β*-D-1-thiogalactopyranoside (IPTG), 4-(2-hydroxyethyl)piperazine-1-ethanesulfonic acid (HEPES), and NaCl were purchase from Formedium. $(NH_4)_2SO_4$ was purchased from Fisher Scientific, and 3-oxovalerate was from Carbosynth. Tobacco etch virus protease (TEVP) was produced as previously described.[1]

Expression of Psychrobacter arcticus HBDH (PaHBDH) and Acinetobacter baumannii HBDH (AbHBDH). The DNA encoding *Pa*HBDH, purchased as a g-Block (IDT Integrated DNA Technologies), was amplified by the polymerase chain reaction (PCR) using the forward primer 5′-CTTTATTTTCAGCATATGGCCACCCAGCTTCAACAAGACT-3′ and the reverse primer 5′-CCCAAGCTTTCAATTCATAAACCAGCCG-3′. The DNA encoding *Ab*HBDH with a TEVP-cleavable N-terminal His-tag, purchased as a g-Block (IDT Integrated DNA Technologies), was amplified by PCR using the forward primer 5′-GGAATTCCATATGCATCATCACCATCATCACG-3′ and the reverse primer 5′-CCAAGCTTTCATTGCGCTGTGTATCC-3′. Both g-blocks were codon-optimised for expression in *Escherichia coli*. The amplified DNA fragments were digested with *Nde*I and *Hin*dIII restriction enzymes and ligated into *Nde*I/*Hin*dIII linearized pJexpress411 vector. The resulting plasmids were sequenced (Eurofins Genomics) to confirm insertion of the gene and that no mutations were introduced. The pJexpress411-*Pa*HBHD expression construct was transformed into *E. coli* BL21 (DE3) competent cells, whereas the pJexpress411-*Ab*HBDH construct was transformed into *E. coli* BL21 (DE3) Gold competent cells. The transformed cells were grown in 1 L of lysogeny broth (LB) containing 50 μg mL^{-1} kanamycin at 37 °C to an optical density at 600 nm (OD_{600nm}) of 0.6. For *Pa*HBDH expression, the culture was equilibrated to 16 °C, while for *Ab*HBDH, the culture was kept at 37 °C, and expression was induced with 0.5 mM IPTG. Cells were allowed to grow for an additional 20-h, harvested by centrifugation at 6774 *g* for 15 min and stored at –20 °C.

Purification of PaHBDH. All purification procedures were performed at 4 °C and all chromatographic steps employed an AKTA Start FPLC system (GE Lifesciences). Cells were thawed on ice for 20 min before being resuspended in buffer A [50 mM HEPES (pH 7.5)] containing 0.2 mg mL^{-1} lysozyme, 0.05 mg mL^{-1} DNase I, and half a tablet of EDTA-free protease inhibitor cocktail, disrupted in a high-pressure cell disruptor (Constant Systems), and centrifuged at 48000 *g* for 30 min to remove cell debris. Buffer A containing 1.5 M $(NH_4)_2SO_4$ was added dropwise to the supernatant, which was stirred for 30 min and centrifuged at 48000 *g* for 30 min to remove the precipitate. The supernatant was dialysed against 3 × 2 L of buffer A, filtered through a 0.45-μm membrane and loaded onto a HiTrap Q FF column (GE Healthcare), pre-equilibrated with buffer A. The column was washed with 15 column volumes (CV) of 5% buffer B [50 mM HEPES, 2 M NaCl (pH 7.5)], and the adsorbed proteins were eluted with 20 CV of a linear gradient from 5 to 20% buffer B. Fractions containing the desired protein were pooled and dialyzed against 3 × 2 L of buffer C [50 mM HEPES (pH 6.5)], filtered through a 0.45-μm membrane and loaded onto a HiTrap Blue HP column (GE Healthcare) pre-equilibrated with buffer C. The flow through was collected and loaded onto a HiTrap Q HP column (GE Healthcare) pre-equilibrated with buffer C. The column was washed with 20 CV of 5% buffer D [50 mM HEPES, 500 mM NaCl (pH 6.5)], and the adsorbed proteins were eluted with 20 CV of 31% buffer D. Fractions containing the desired protein were pooled and dialyzed against 2 × 2 L of buffer E [50 mM HEPES, 1.5 M $(NH_4)_2SO_4$ (pH 6.5)], filtered through a 0.45-μm membrane and loaded onto a HiTrap Phenyl Sepharose column (GE Healthcare) pre-equilibrated with buffer E. The column was washed with 10 CV of 25% buffer A, and the adsorbed proteins were eluted with a linear gradient from 25 to 53% buffer A. Fractions were analysed by sodium dodecyl sulphate−polyacrylamide gel electrophoresis (SDS−PAGE) (NuPAGE Bis-Tris 4−12% Precast gels, Thermo Fisher Scientific), pooled, concentrated using 10000-molecular-weight-cut-off (MWCO) ultrafiltration membranes (Millipore), dialyzed against 2 × 2 L of 20 mM HEPES (pH 8.0), aliquoted, and stored at −80 °C. The concentration was determined spectrophotometrically (NanoDrop) at 280 nm using the theoretical extinction coefficient (ε_{280}) of 16960 M^{-1} cm^{-1}. The molecular mass was determined by electrospray ionization mass spectrometry (ESI-MS).

Purification of AbHBDH. All purification procedures were performed at 4 °C and all chromatographic steps employed an AKTA Start FPLC system (GE Lifesciences). Cells were allowed to thaw on ice for 20 min before being resuspended in buffer A [50 mM HEPES, 300 mM NaCl, 10 mM imidazole, (pH 8.0)] containing 0.2 mg mL^{-1} lysozyme, 0.05 mg mL^{-1} DNase I, and half a tablet of EDTA-free Cømplete protease inhibitor cocktail, disrupted in a high-pressure cell disruptor (Constant Systems), and centrifuged at 48000 *g* for 30 min to remove cell debris. The supernatant was filtered through a 0.45-μm membrane and loaded onto a HisTrap FF column (GE Healthcare) pre-equilibrated with buffer A. The column was washed with 10 CV of buffer A, and the adsorbed proteins were eluted with 20 CV of a linear gradient from 0 to 100% buffer B [50 mM HEPES, 300 mM imidazole, 300 mM NaCl (pH 8.0)]. Fractions containing the desired protein were pooled, mixed with TEVP (1 mg of TEVP to 15 mg of *Ab*HBDH) and dialyzed against 2 × 2 L of buffer C [20 mM HEPES, 150 mM NaCl, 2 mM DTT, 10% glycerol (*v/v*), (pH 7.5)], 2 × 2 L of buffer D [20 mM HEPES, (pH 8)], and 1 × 2 L of buffer A. Samples were filtered through a 0.45-μm membrane and loaded onto a HisTrap FF (GE Healthcare) pre-equilibrated with buffer A. The flow through was collected and analysed by SDS−PAGE (NuPAGE Bis-Tris 4−12% Precast gels, Thermo Fisher Scientific), concentrated using 10000-MWCO ultrafiltration membranes (Millipore), dialyzed against 2 × 2 L of buffer D, aliquoted, and stored at −80 °C. The concentration was determined spectrophotometrically (NanoDrop) at 280 nm using the theoretical extinction coefficient (ε_{280}) of 8940 M^{-1} cm^{-1}. The molecular mass was determined by ESI-MS.

PaHBDH and AbHBDH substrate saturation curves. Assays (500 μL) were performed under initial rate conditions in 100 mM HEPES (pH 7.0), and reactions were started by the addition of NADH after 3 min incubation at each temperature. Reaction rates were measured in a Shimadzu UV 2600 spectrophotometer by monitoring the decrease in absorbance at 340 nm (ε = 6220 M^{-1} cm^{-1}), 370 nm (ε = 2320 M^{-1} cm^{-1}), or 380 nm (ε = 1210 M^{-1} cm^{-1}) due to the oxidation of NADH, in 1-cm optical path length quartz cuvettes (Hellma). All measurements were performed in at least duplicate.

*Pa*HBDH initial rates with acetoacetate were measured at various temperatures (283 – 318 K) in the presence of 5 nM (283 – 303 K), or 2.5 nM (308 – 318 K) *Pa*HBDH, saturating concentrations of one substrate, and varying concentrations of the other: acetoacetate (0.025 – 0.4 mM, 283 – 293 K; 0.05 – 0.8 mM, 298 – 313 K; 0.1 – 1.6 mM, 318 K) and NADH (0.01 – 0.16 mM, 283 – 298 K; 0.02 – 0.32 mM, 303 –318 K). *Pa*HBDH initial rates with 3-oxovalerate were measured at various temperatures (283 – 318 K) in the presence of 10 nM (283 – 288 K), 20 nM (293 K, 313 – 318 K), or 30 nM (298 – 308 K) *Pa*HBDH, saturating concentrations of one substrate, and varying concentrations of the other: 3-oxovalerate (0.0125 – 0.2 mM, 283K; 0.025 – 0.4 mM, 288 – 318 K) and NADH (6.25 x 10^{-4} – 0.01 mM, 283 K; 0.00125 – 0.02 mM, 288 K; 0.0025 – 0.04 mM, 293 K; 0.05 – 0.08 mM, 298 – 318 K).

*Ab*HBDH initial rates with acetoacetate were measured at various temperatures (283 – 330 K) in the presence of 50 nM (283 – 293 K), 16 nM (298 – 323 K), or 32 nM (328 – 330 K) *Ab*HBDH, saturating concentrations of one substrate, and varying concentrations of the other: acetoacetate (0.05 – 0.8 mM, 283 – 323 K; 0.1 – 1.6 mM, 323 – 330 K) and NADH (0.02 – 0.32 mM, 283 – 318 K; 0.04 – 0.64 mM, 323 K; 0.08 – 1.28 mM, 325 – 330 K). *Ab*HBDH initial rates with 3-oxovalerate were measured at various temperatures (283 – 330 K) in the presence of 576 nM (283 K), 480 nM (288 – 308 K), 384 nM (313 – 318 K), 288 nM (323 – 328 K), or 240 nM (330 K) *Ab*HBDH, saturating concentrations of one substrate, and varying concentrations of the other: 3-oxovalerate (0.025 – 0.4 mM, 283 – 330 K) and NADH (0.01 – 0.16 mM, 283 – 298 K; 0.02 – 0.32 mM, 303 – 318 K; 0.04 – 0.64 mM, 323 – 330 K). To ensure that enzyme activities were stable at these temperatures for the duration of the assay, *Pa*HBDH and *Ab*HBDH were incubated at the extremes of their respective experimental temperature ranges and subsequently assayed at 298 K, with no loss of activity occurring upon incubation for at least 5 min.

PaHBDH and AbHBDH saturation kinetics in glycerol. *Pa*HBDH (2.5 nM) initial rates with acetoacetate were measured at 298 K at saturating concentrations of one substrate and varying concentrations of the other, either acetoacetate (0.05 – 0.8 mM) in the presence of 0%, 18%, and 27% glycerol (*v/v*), or NADH (0.005 – 0.08 mM, 0% and 18% glycerol; 0.01 – 0.16 mM, 27% glycerol). For

the experiments using 3-oxovalerate, the rates were measured in the presence of 50 nM *Pa*HBDH, saturating concentrations of one substrate and varying concentrations of the other: 3-oxovalerate (0.025 – 0.4 mM) in the presence of 0%, 18%, and 27% glycerol (*v/v*), and NADH (0.005 – 0.08 mM, 0% and 18% glycerol; 0.01 – 0.16 mM, 27% glycerol). *Ab*HBDH (50 nM) initial rates were measured at 298 K at saturating concentrations of one substrate and varying concentrations of the other, either acetoacetate (0.05 – 0.8 mM, 0% glycerol; 0.025 – 0.4 mM, 18% and 27% glycerol) or NADH (0.02 – 0.32 mM), in the presence of 0%, 18%, and 27% glycerol (*v/v*). The same methodology was used for the 3-oxovalerate, where initial rates in the presence of 480 nM *Ab*HBDH were measured at varying concentrations of 3-oxovalerate (0.025 – 0.4 mM), and NADH (0.01 – 0.16 mM) in the presence of 0%, 18%, and 27% glycerol (*v/v*). All measurements were performed in at least duplicate.

*PaHBDH and AbHBDH saturation kinetics in PEG-8000. Pa*HBDH (2.5 nM) initial rates were measured at 298 K at saturating concentrations of one substrate and varying concentrations of the other, either acetoacetate (0.05 – 0.8 mM) or NADH (0.01 – 0.16 mM) in the presence of 0% and 5% PEG-8000 (*w/v*). *Ab*HBDH (50 nM) initial rates were measured at 298 K at saturating concentrations of one substrate and varying concentrations of the other, either acetoacetate (0.05 – 0.8 mM) or NADH (0.02 – 0.32 mM) in the presence of 0% and 5% PEG-8000 (*w/v*). All measurements were performed in at least duplicate.

PaHBDH and AbHBDH thermal denaturation by differential scanning fluorimetry (DSF). DSF measurements (λ_{ex} = 490 nm, λ_{em} 610 nm) were performed in a 96-well plate on a Stratagene Mx3005p instrument. Thermal denaturation assays (50 µL) for 5 µM *Pa*HBDH and *Ab*HBDH were measured in the presence and absence of ligands (5 mM acetoacetate, 5 mM NAD^+, 5 mM NADH, 5 mM 3-oxovalerate) in 100 mM HEPES, pH 7.0. Sypro Orange (5×) (Invitrogen) was added to all wells. Thermal denaturation curves were recorded over a temperature range from 25 – 93 °C with 1 °C min^{-1} increments. Control curves lacking enzyme were subtracted from curves containing enzyme. All measurements were carried out in triplicate.

Pre-steady-state kinetics. All reactions were carried out in 100 mM HEPES (pH 7.0) by monitoring the decrease of NADH at 340 nm (283 K, 298 K and 318 K) or 370 nm (328 K) in an Applied Photophysics SX-20 stopped-flow spectrofluorimeter outfitted with a xenon lamp, a 5-μL mixing cell (0.5-cm path length and 0.9-ms dead-time) and a circulating water bath for temperature control.

Multiple-turnover rates were measured at saturating concentrations of both substrates. For *Pa*HBDH (25 μM), at 283 K, 0.75 mM acetoacetate and 0.25 mM NADH or 0.25 mM 3-oxovalerate and 0.25 mM NADH; at 298 K, 1 mM acetoacetate and 0.85 mM NADH or 0.4 mM 3-oxovalerate and 0.7 mM NADH; at 318 K, 5.25 mM acetoacetate and 0.5 mM NADH or 1.95 mM 3-oxovalerate and 0.25 mM NADH. For *Ab*HBDH (50 μM), at 283 K, 2.1 mM acetoacetate and 1.05 mM NADH or 1.35 mM 3-oxovalerate and 0.5 mM NADH; at 298 K, 1 mM acetoacetate and 0.85 mM NADH or 0.9 mM 3-oxovalerate and 0.9 mM NADH; at 328 K, 5 mM acetoacetate and 2.25 mM NADH or 1.35 mM 3-oxovalerate and 2.25 mM NADH. Enzyme and NADH were kept in one syringe while the other substrate was kept in the second syringe. Reaction was triggered by rapidly mixing 55 μL from each syringe. A minimum of 6 traces with 5000 data-points per trace were collected for each enzyme at each temperature.

Single-turnover rates of *Pa*HBDH were measured at saturating concentrations of either acetoacetate (283 K, 0.75 mM; 298 K, 1.65 mM) or 3-oxovalerate (283 K, 0.75 mM; 298 K, 0.6 mM), 4 μM NADH and excess concentrations of enzyme (40 μM and 50 μM). *Pa*HBDH was kept in one syringe and substrates in another syringe. For *Ab*HBDH, single-turnover rates were measured at saturating concentrations of either acetoacetate (283 K and 298 K, 2.1 mM) or 3-oxovalerate (283 K, 0.85 mM; 298 K, 2.5 mM), NADH (283 K, 4 μM; 298 K, 5 μM) and excess concentrations of enzyme (283 K, 40 μM and 60 μM; 298 K, 80 μM and 160 μM). *Ab*HBDH and NADH was kept in one syringe and the other substrate in another syringe. Reaction was triggered by rapidly mixing 55 μL from each syringe. A minimum of 6 traces with 5000 data-points per trace were collected for each enzyme at each

temperature. In all cases, the enzyme concentration was at least 10-fold higher than the NADH concentration, and pseudo-first order approximation was assumed.

Kinetic and thermal denaturation data analysis. Kinetic data were analysed by the nonlinear regression function of SigmaPlot 14 (SPSS Inc.). Data points and error bars in graphs represent mean ± standard error, and kinetic and equilibrium constants are presented as mean ± fitting error. Substrate saturation curves were fitted to eq S1 where v is the initial rate, E_T is total enzyme concentration, S is the concentration of the varying substrate, k_{cat} is the steady-state turnover number, and K_M is the Michaelis constant.

$$\frac{v}{E_T} = \frac{k_{cat}S}{K_M+S} \qquad \text{eq S1}$$

DSF thermal denaturation data were fitted to eq S2, where F_U is fraction unfolded, T is the temperature in K, T_m is the melting temperature, c is the slope of the transition region, and LL and UL are folded and unfolded baselines, respectively.[2]

$$F_U = LL + \frac{UL-LL}{1+e^{(T_m-T)/c}} \qquad \text{eq S2}$$

Pre-steady-state multiple- and single-turnover data were fitted to eqs S3 and S4, respectively, where $[NADH]_t$ is the concentration of NADH at time t, $[NADH]_{t0}$ is the NADH concentration at time zero, $[NADH]_\infty$ is the NADH concentration as time approaches infinity, A_0 is the amplitude change, t is the reaction time, v is the initial velocity, and k_{STO} is the single-turnover rate constant.

$$[NADH]_t = [NADH]_{t0} + vt \qquad \text{eq S3}$$

$$[NADH]_t = [NADH]_\infty + A_0 e^{-k_{STO}t} \qquad \text{eq S4}$$

Solvent viscosity effects on k_{cat} were fitted to eq S5, where $k_{cat\,0}$ and $k_{cat\,\eta}$ are k_{cat} in the presence and absence of glycerol, respectively, η_{rel} is the relative viscosity of the solution, and m is the slope.

$$\frac{k_{cat\,0}}{k_{cat\,\eta}} = m(\eta_{rel} - 1) + 1 \qquad \text{eq S5}$$

Scheme S1. HBDH-Catalysed Reaction.

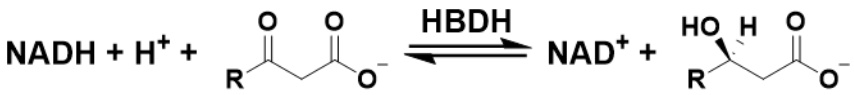

R = CH_3: Acetoacetate and 3-hydroxybutyrate
R = CH_2CH_3: 3-Oxovalerate and 3-hydroxyvalerate

RESULTS

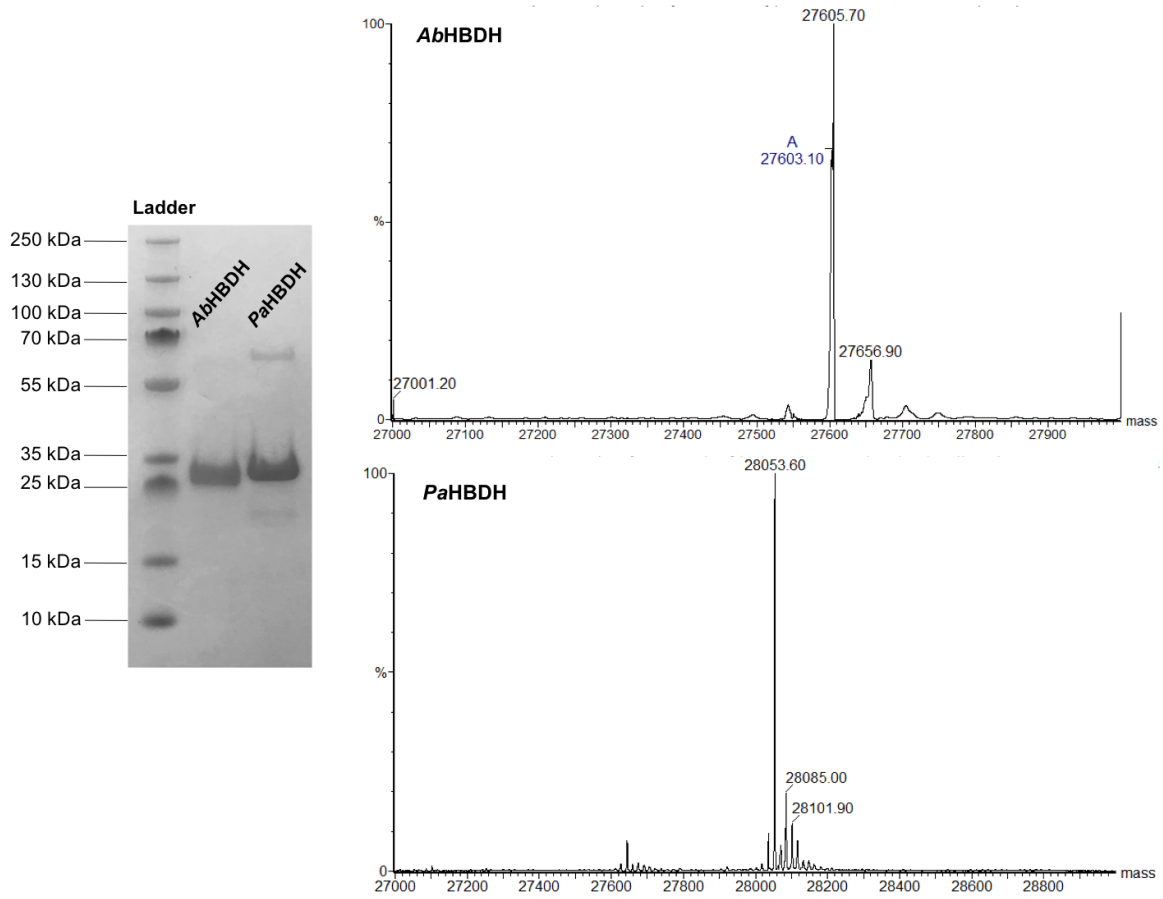

Figure S1. Purification of *Ab*HBDH and *Pa*HBDH. *Left*, SDS PAGE, with protein ladder, *Ab*HBDH after the second HisTrap FF column, *Pa*HBDH after the HiTrap Phenyl Sepharose column. *Right*, ESI mass-spectrometry analysis showing the experimentally determined mass of 27605.7 for *Ab*HBDH (*top*), consistent with *Ab*HBDH having an additional glycine at the N-terminus, as expected following His-tag removal by TEVP, and 28053.6 for *Pa*HBDH (*bottom*), showing the molecular mass of the protein is 132 units lower than the predicted value of 28183, in agreement with the loss of the N-terminal methionine.

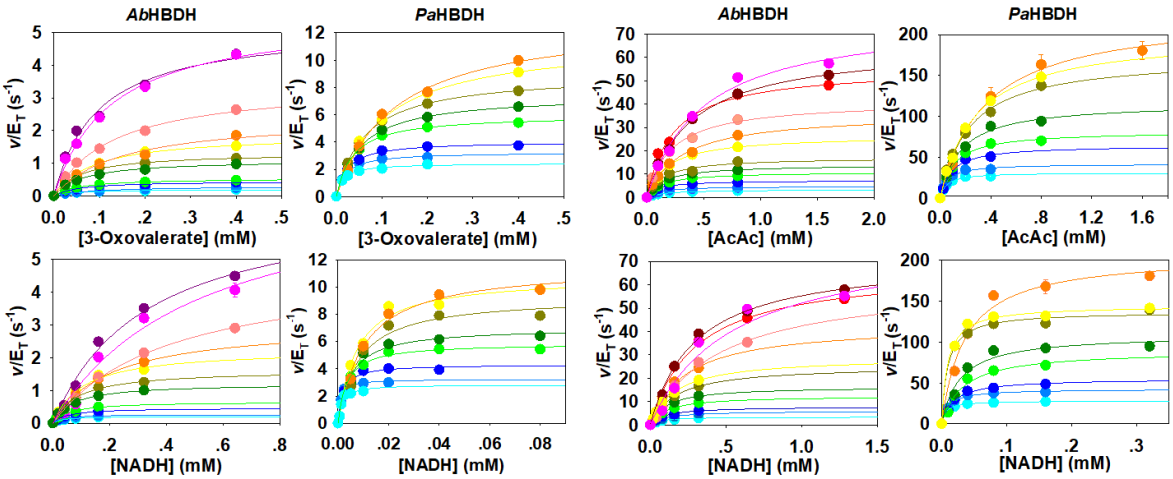

Figure S2. Substrate saturation curves for *Ab*HBDH and *Pa*HBDH over several temperatures. Temperature ranges are 283 K – 330 K for *Ab*HBDH reactions, and 283 K – 318 K for *Pa*HBDH reactions. Data are mean ± SE from at least duplicate measurements, and lines are data fitting to eq S1.

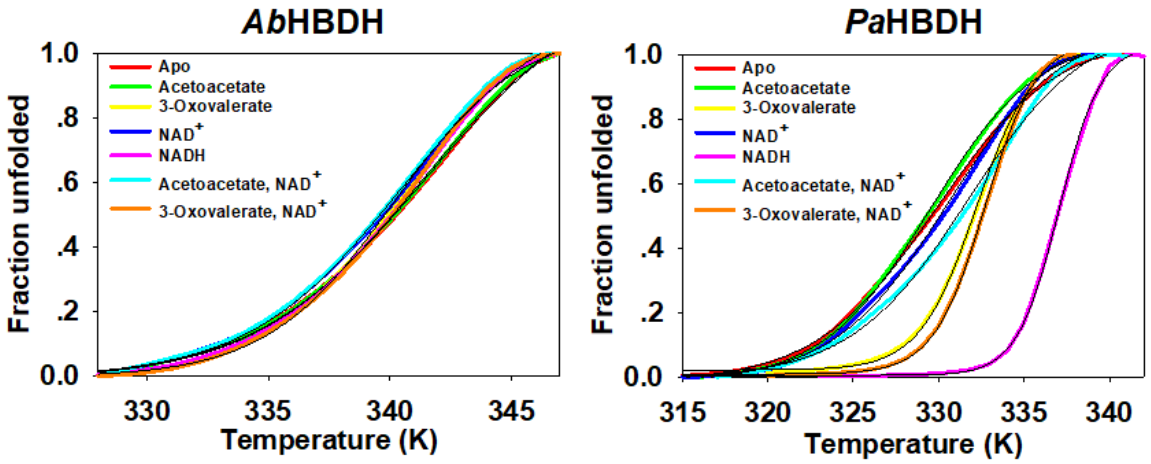

Figure S3. Thermal denaturation curves from DSF for *Ab*HBDH and *Pa*HBDH in the absence and presence of ligands. Black lines represent the data fitting to eq S2.

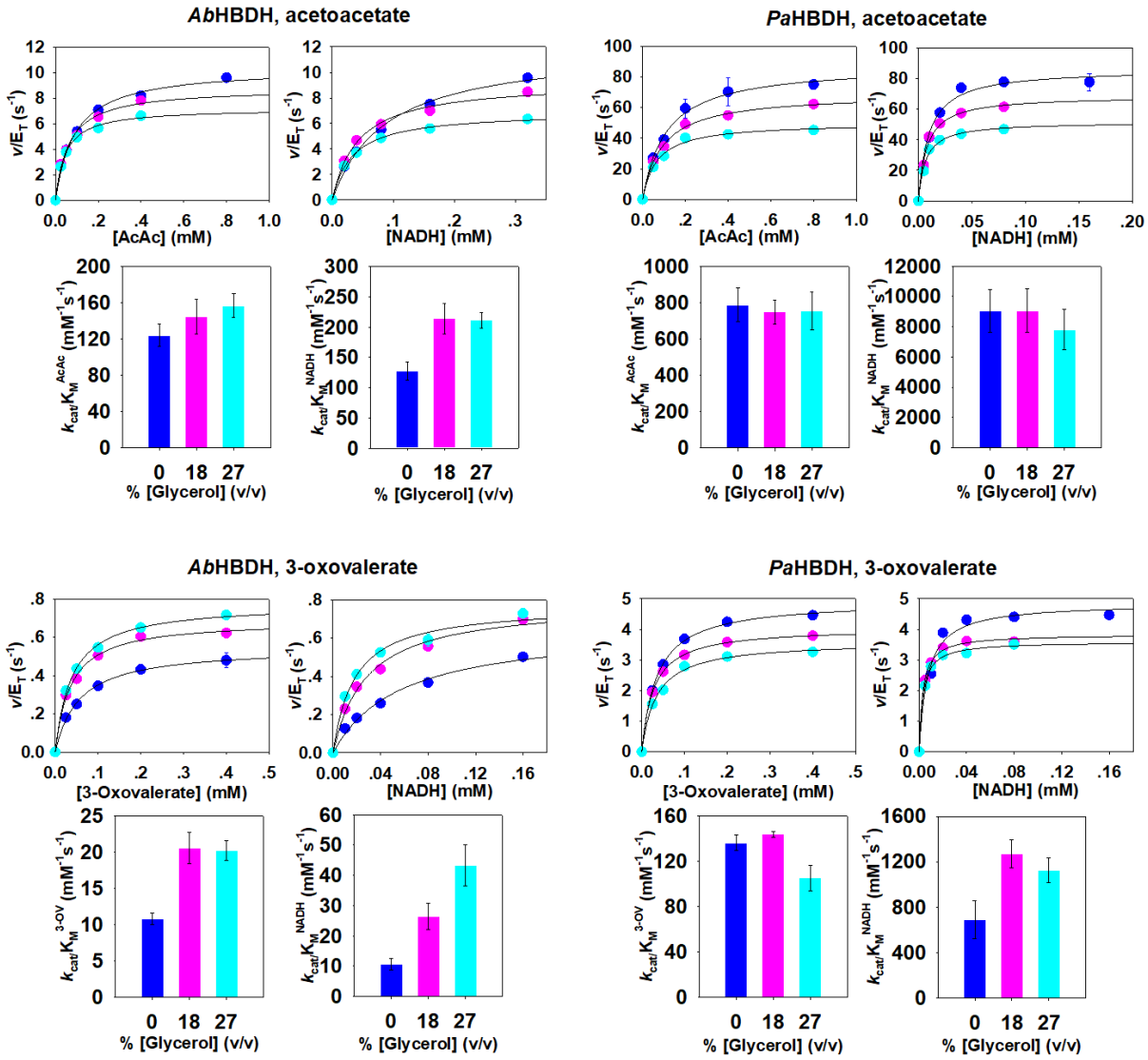

Figure S4. Solvent viscosity studies with *Ab*HBDH (*left*) and *Pa*HBDH (*right*) in 0% glycerol (blue), 18% glycerol (pink) and 27% glycerol (cyan). The scatter plots are substrate saturation curves where data represent mean ± SE from at least duplicate measurements, and lines are data fitting to eq S1. The bar plots show the effect of glycerol on the second-order rate constants and represent value ± fitting error obtained upon substrate saturation data fitting to eq S1.

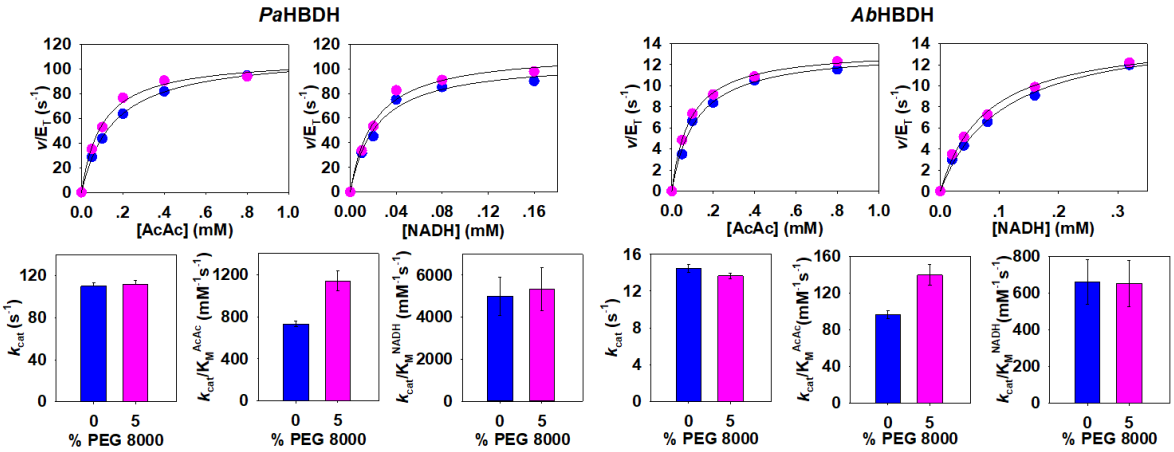

Figure S5. Solvent macroviscosity studies for acetoacetate reduction catalysed by *Pa*HBDH (*left*) and *Ab*HBDH (*right*) in 0% PEG-8000 (blue) and 5% PEG-8000 (pink). The scatter plots are substrate saturation curves where data represent mean ± SE from at least duplicate measurements, and lines are data fitting to eq S1. The bar plots show the effect of PEG-8000 on steady-state rate constants and represent value ± fitting error obtained upon substrate saturation data fitting to eq S1.

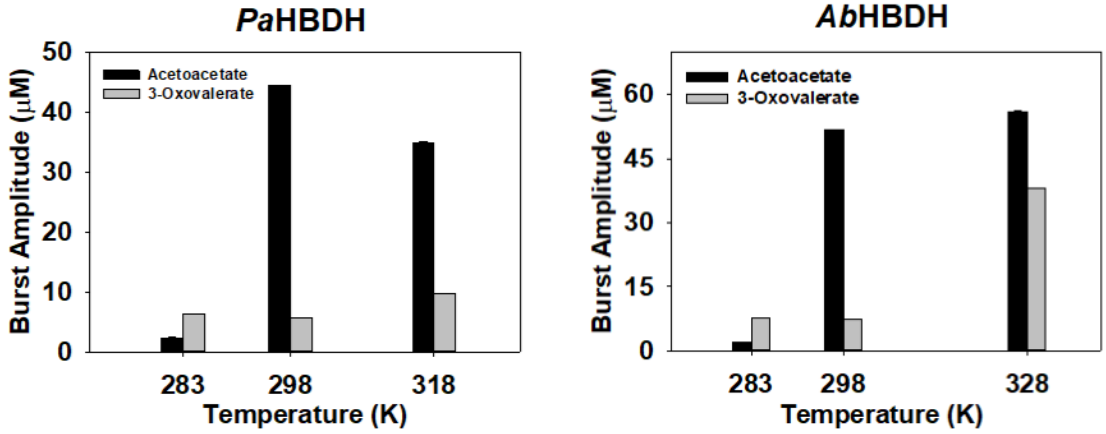

Figure S6. Pre-steady-state multiple-turnover burst amplitude inferred from the NADH concentration offset in the presence and absence of the co-substrate at time zero. The amplitudes were calculated from the data shown in Figures 3 and 5.

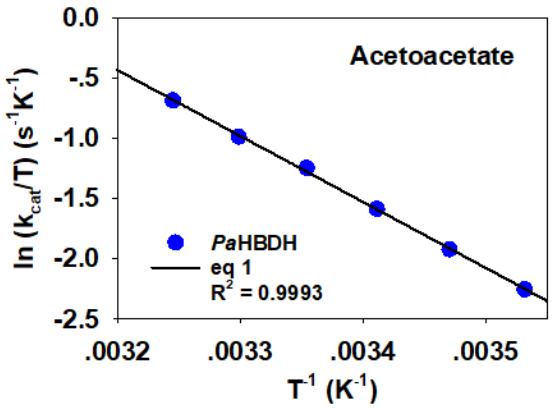

Figure S7. Eyring plot for *Pa*HBDH-catalysed reduction of acetoacetate in the temperature range of 283 K – 308 K. Data represent mean ± SE of at least duplicate measurements, and line is data fitting to eq 1.

Simulated Eyring plots for microscopic and macroscopic rate constants. To illustrate the kinetic complexity underlying both linear and nonlinear Eyring plots for macroscopic rate constants, and the caution that must be wielded when attempting to interpret them in terms of specific steps in an enzyme reaction, Eyring plots were simulated (Figure S8) for two hypothetical microscopic rate constants (k_3 and k_5) and the resulting macroscopic rate constant (k_{cat}) for a simple two-step mechanism (Scheme S2).

Scheme S2. A hypothetical two-step mechanism for an enzyme reaction.

$$ES \xrightarrow{k_3} EP \xrightarrow{k_5} E + P$$

In Scheme S2, k_3 is the microscopic rate constant for the chemical step, and k_5 is the microscopic rate constant for product release from the enzyme. ES, EP, E and P are the enzyme-substrate complex, enzyme-product complex, free enzyme, and free product, respectively. Since the macroscopic rate constant of interest is k_{cat}, the mechanism starts with the substrate-saturated enzyme.

$$k_{cat} = \frac{k_3 k_5}{k_3 + k_5} \quad \text{eq S6}$$

To generate the simulated Eyring plots, arbitrary values of k_3 and k_5 were chosen so that plots of ln (k/T) *vs* 1/T (283 K – 318 K) would be linear. These linear plots were made to intercept one another to reflect a change in rate-limiting step from k_3 at low temperatures to k_5 at high temperatures. From the values of k_3 and k_5, k_{cat} values were calculated using eq S6, and plotted as ln (k/T) *vs* 1/T. Eyring plots for k_3 and k_5 were fitted to eq 1, while Eyring plots for k_{cat} were fitted to both eqs 1 and 2.

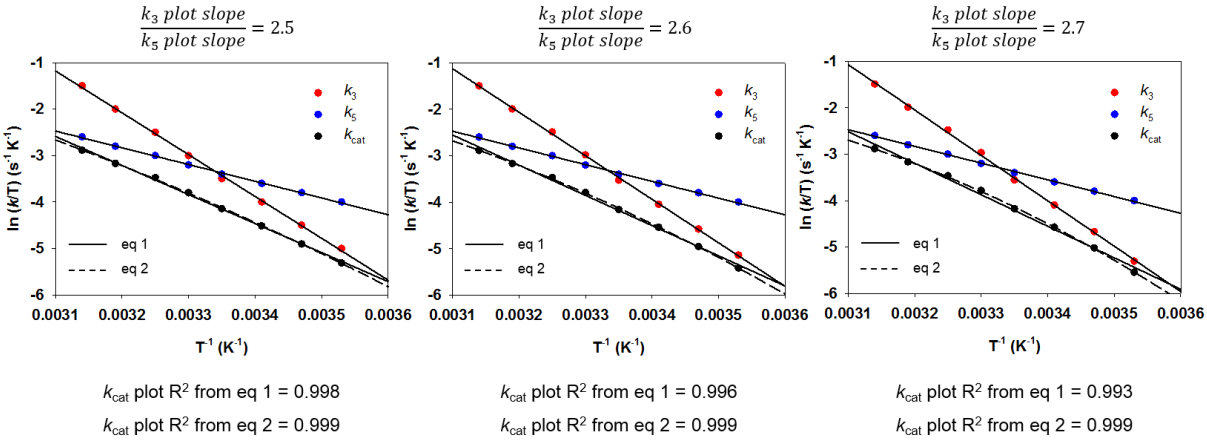

Figure S8. Simulated linear Eyring plots for microscopic rate constants k_3 and k_5, and the resulting Eyring plot for k_{cat}. The ratio of slopes of Eyring plots for k_3 and k_5 increases from left to right.

For this simple two-step mechanism, a ratio of slopes of Eyring plots for k_3 and k_5 (which is a ratio of the $\Delta H^{\ddagger}$ for each step) of 2.5, where a clear change in rate-limiting step from k_3 at low temperatures to k_5 at high temperatures takes place, still produces a linear Eyring plot for k_{cat} whose fitting to eqs 1 and 2 are virtually indistinguishable (Figure S8, *left*). A deviation from linearity in the k_{cat} Eyring plot only becomes noticeable once the ratio of slopes of Eyring plots for k_3 and k_5 reaches 2.6 (Figure S8, *middle*), and can be clearly seen when that ratio increases to 2.7 (Figure S8, *right*). Obviously this would become more complex if the mechanism involved more steps. Therefore, when generating temperature-rate profiles of k_{cat}, one should not probe the reaction for a temperature-dependent change in rate-limiting step only when a nonlinear Eyring plot is obtained.

Table S1. Steady-state kinetic constants for *Ab*HBDH-catalysed acetoacetate reduction at different temperatures.[a]

Parameter	k_{cat} (s^{-1})	K_M^{AcAc} (mM)	K_M^{NADH} (mM)	k_{cat}/K_M^{AcAc} (M^{-1} s^{-1})	k_{cat}/K_M^{NADH} (M^{-1} s^{-1})
283 K	3.4 ± 0.1	0.14 ± 0.01	0.07 ± 0.01	$2.4 \pm 0.2 \times 10^4$	$5.1 \pm 0.1 \times 10^4$
288 K	5.3 ± 0.2	0.096 ± 0.004	0.09 ± 0.01	$5.6 \pm 0.3 \times 10^4$	$5.5 \pm 0.8 \times 10^4$
293 K	7.6 ±0.2	0.09 ± 0.01	0.09 ± 0.01	$8.1 \pm 0.5 \times 10^4$	$7.9 \pm 1 \times 10^4$
298 K	11.7 ± 0.3	0.13 ± 0.01	0.11 ± 0.01	$8.9 \pm 0.6 \times 10^4$	$1.1 \pm 0.1 \times 10^5$
303 K	15.2 ± 0.1	0.146 ± 0.004	0.107 ± 0.004	$1.04 \pm 0.03 \times 10^5$	$1.4 \pm 0.05 \times 10^5$
308 K	21.3 ± 0.9	0.14 ± 0.03	0.17 ± 0.02	$1.5 \pm 0.3 \times 10^5$	$1.2 \pm 0.1 \times 10^5$
313 K	27.8 ± 0.9	0.18 ± 0.02	0.17 ± 0.01	$1.5 \pm 0.2 \times 10^5$	$1.6 \pm 0.2 \times 10^5$
318 K	39 ± 3	0.31 ± 0.03	0.23 ± 0.07	$1.3 \pm 0.2 \times 10^5$	$1.7 \pm 0.5 \times 10^5$
323 K	52 ± 4	0.22 ± 0.02	0.5 ± 0.1	$2.4 \pm 0.3 \times 10^5$	$1.1 \pm 0.3 \times 10^5$
325 K	61 ± 2	0.23 ± 0.03	0.30 ± 0.04	$2.6 \pm 0.3 \times 10^5$	$2.1 \pm 0.3 \times 10^5$
328 K	69 ± 3	0.39 ± 0.03	0.30 ± 0.03	$1.8 \pm 0.2 \times 10^5$	$2.3 \pm 0.2 \times 10^5$
330 K	79 ± 7	0.5 ± 0.1	0.5 ± 0.2	$1.6 \pm 0.3 \times 10^5$	$1.6 \pm 0.6 \times 10^5$

[a]Values represent mean ± fitting error of at least duplicate measurements.

Table S2. Steady-state kinetic constants for *Pa*HBDH-catalysed acetoacetate reduction at different temperatures.[a]

Parameter	k_{cat} (s^{-1})	K_M^{AcAc} (mM)	K_M^{NADH} (mM)	k_{cat}/K_M^{AcAc} (M^{-1} s^{-1})	k_{cat}/K_M^{NADH} (M^{-1} s^{-1})
283 K	30 ± 1	0.05 ± 0.01	0.0064 ± 0.0002	$6.3 \pm 0.8 \times 10^5$	$4.6 \pm 0.2 \times 10^6$
288 K	42 ± 1	0.06 ± 0.01	0.010 ± 0.001	$7.8 \pm 1.1 \times 10^5$	$4.1 \pm 0.5 \times 10^6$
293 K	60 ± 3	0.09 ± 0.02	0.019 ± 0.003	$6.6 \pm 1.2 \times 10^5$	$3.2 \pm 0.6 \times 10^6$
298 K	86 ± 4	0.11 ± 0.01	0.03 ± 0.01	$8.0 \pm 0.9 \times 10^5$	$2.7 \pm 0.7 \times 10^6$
303 K	112 ± 5	0.16 ± 0.02	0.03 ± 0.01	$6.9 \pm 0.9 \times 10^5$	$4.0 \pm 1.1 \times 10^6$
308 K	155 ± 4	0.23 ± 0.02	0.009 ± 0.002	$6.7 \pm 0.7 \times 10^5$	$1.7 \pm 0.3 \times 10^7$
313 K	172 ± 3	0.28 ± 0.02	0.009 ± 0.001	$6.2 \pm 0.5 \times 10^5$	$1.9 \pm 0.3 \times 10^7$
318 K	216 ± 8	0.35 ± 0.05	0.04 ± 0.01	$6.2 \pm 0.9 \times 10^5$	$6.1 \pm 1.1 \times 10^7$

[a]Values represent mean ± fitting error of at least duplicate measurements.

Table S3. Steady-state kinetic constants for *Ab*HBDH-catalysed 3-oxovalerate reduction at different temperatures.[a]

Parameter	k_{cat} (s^{-1})	$K_M^{3\text{-OV}}$ (mM)	K_M^{NADH} (mM)	$k_{cat}/K_M^{3\text{-OV}}$ ($M^{-1}\ s^{-1}$)	k_{cat}/K_M^{NADH} ($M^{-1}\ s^{-1}$)
283 K	0.21 ± 0.01	0.05 ± 0.01	0.031 ± 0.009	$3.8 \pm 0.8 \times 10^3$	$6.7 \pm 1.9 \times 10^3$
288 K	0.28 ± 0.01	0.09 ± 0.01	0.031 ± 0.006	$3.2 \pm 0.5 \times 10^3$	$9.3 \pm 1.8 \times 10^3$
293 K	0.46 ± 0.02	0.05 ± 0.01	0.051 ± 0.008	$8.6 \pm 1.6 \times 10^3$	$9.1 \pm 1.5 \times 10^3$
298 K	0.60 ± 0.03	0.056 ± 0.003	0.07 ± 0.01	$1.1 \pm 0.08 \times 10^4$	$1.1 \pm 0.2 \times 10^4$
303 K	1.16 ± 0.02	0.065 ± 0.006	0.070 ± 0.005	$1.8 \pm 0.2 \times 10^4$	$1.7 \pm 0.1 \times 10^4$
308 K	1.47 ± 0.03	0.059 ± 0.004	0.088 ± 0.007	$2.5 \pm 0.2 \times 10^4$	$1.7 \pm 0.1 \times 10^4$
313 K	2.07 ± 0.09	0.087 ± 0.007	0.10 ± 0.02	$2.4 \pm 2 \times 10^4$	$2.0 \pm 0.4 \times 10^4$
318 K	2.7 ± 0.1	0.15 ± 0.04	0.20 ± 0.01	$1.8 \pm 0.4 \times 10^4$	$1.4 \pm 0.1 \times 10^4$
323 K	4.1 ± 0.2	0.13 ± 0.01	0.41 ± 0.06	$3.1 \pm 0.4 \times 10^4$	$1.0 \pm 0.1 \times 10^4$
328 K	6.1 ± 0.4	0.10 ± 0.02	0.33 ± 0.07	$6.3 \pm 1.2 \times 10^4$	$1.8 \pm 0.4 \times 10^4$
330 K	6.6 ± 0.9	0.12 ± 0.01	0.5 ± 0.2	$5.3 \pm 1.0 \times 10^4$	$1.3 \pm 0.6 \times 10^4$

[a]Values represent mean ± fitting error of at least duplicate measurements.

Table S4. Steady-state kinetic constants for *Pa*HBDH-catalysed 3-oxovalerate reduction at different temperatures.[a]

Parameter	k_{cat} (s^{-1})	$K_M^{3\text{-OV}}$ (mM)	K_M^{NADH} (mM)	$k_{cat}/K_M^{3\text{-OV}}$ ($M^{-1}\ s^{-1}$)	k_{cat}/K_M^{NADH} ($M^{-1}\ s^{-1}$)
283 K	2.6 ± 0.2	0.014 ± 0.001	0.002 ± 0.001	$1.8 \pm 0.2 \times 10^5$	$1.8 \pm 0.02 \times 10^6$
288 K	3.2 ± 0.1	0.020 ± 0.002	0.0009 ± 0.0002	$1.6 \pm 0.4 \times 10^5$	$3.6 \pm 0.04 \times 10^6$
293 K	4.2 ± 0.1	0.024 ± 0.002	0.0018 ± 0.0003	$1.8 \pm 0.5 \times 10^5$	$2.3 \pm 0.05 \times 10^6$
298 K	5.9 ± 0.1	0.036 ± 0.002	0.0034 ± 0.0004	$1.6 \pm 0.8 \times 10^5$	$1.7 \pm 0.8 \times 10^6$
303 K	7.2 ± 0.2	0.054 ± 0.001	0.005 ± 0.001	$1.3 \pm 0.6 \times 10^5$	$1.4 \pm 0.4 \times 10^6$
308 K	9.1 ± 0.3	0.064 ± 0.001	0.008 ± 0.002	$1.4 \pm 0.5 \times 10^5$	$1.1 \pm 0.3 \times 10^6$
313 K	11.1 ± 0.3	0.10 ± 0.01	0.007 ± 0.001	$1.1 \pm 0.3 \times 10^5$	$1.5 \pm 0.3 \times 10^6$
318 K	12.3 ± 0.4	0.13 ± 0.01	0.010 ± 0.002	$9.6 \pm 3.4 \times 10^4$	$1.2 \pm 0.03 \times 10^6$

[a]Values represent mean ± fitting error of at least duplicate measurements.

Table S5. *Ab*HBDH and *Pa*HBDH T_ms (in K) from DSF in the presence and absence of ligands.[a]

Ligand	*Ab*HBDH	*Pa*HBDH
No ligand	341.4 ± 0.2	329.8 ± 0.1
Acetoacetate	341.2 ± 0.1	329.5 ± 0.1
3-Oxovalerate	340.2 ± 0.1	332.19 ± 0.04
NAD^+	340.4 ± 0.2	330.6 ± 0.1
NADH	340.4 ± 0.1	337.04 ± 0.03
Acetoacetate, NAD^+	340.2 ± 0.1	331.8 ± 0.2
3-Oxovalerate, NAD^+	340.3 ± 0.1	332.71 ± 0.03

[a]Values represent mean ± fitting error of triplicate measurements

Table S6. Thermodynamic parameters from Eyring plots fitted to eqs 1 and 2.

Parameter	$\Delta H^{\ddagger}$ (kcal mol^{-1})[a]	R^2 (eq 1)	$\Delta H^{\ddagger}_{T_0}$ (kcal mol^{-1})[b]	$\Delta C_P^{\ddagger}$ (kcal mol^{-1} K^{-1})[b]	R^2 (eq 2)
***Ab*HBDH, Acetoacetate**	11.5 ± 0.1	0.9987	11.9 ± 0.2	– 0.04 ± 0.02	0.9992
***Pa*HBDH, Acetoacetate**	9.7 ± 0.4	0.9879	10.1 ± 0.2	– 0.19 ± 0.05	0.9975
***Ab*HBDH, 3-oxovalerate**	13.2 ± 0.3	0.9960	13.8 ± 0.5	0.003 ± 0.045	0.9963
***Pa*HBDH, 3-oxovalerate**	7.7 ± 0.3	0.9900	8.5 ± 0.3	– 0.09 ± 0.06	0.9945

[a]From eq 1.
[b]From eq 2.

Table S7. Solvent viscosity effects on *Ab*HBDH steady-state kinetic parameters for acetoacetate reduction at 298 K.[a]

Parameter	0% glycerol (*v/v*)	18% glycerol (*v/v*)	27% glycerol (*v/v*)
k_{cat} (s^{-1})	11.2 ± 0.3	9.0 ± 0.2	7.0 ± 0.1
K_M^{AcAc} (mM)	0.090 ± 0.009	0.062 ± 0.008	0.045 ± 0.004
K_M^{NADH} (mM)	0.09 ± 0.01	0.042 ± 0.005	0.033 ± 0.002
k_{cat}/K_M^{AcAc} (M^{-1} s^{-1})	1.2 ± 0.1 × 10^5	1.4 ± 0.2 × 10^5	1.6 ± 0.1 × 10^5
k_{cat}/K_M^{NADH} (M^{-1} s^{-1})	1.3 ± 0.2 × 10^5	2.1 ± 0.3 × 10^5	2.1 ± 0.1 × 10^5

[a]Values represent mean ± fitting error of duplicate measurements.

Table S8. Solvent viscosity effects on *Pa*HBDH steady-state kinetic parameters for acetoacetate reduction at 298 K.[a]

Parameter	0% glycerol (*v/v*)	18% glycerol (*v/v*)	27% glycerol (*v/v*)
k_{cat} (s^{-1})	87 ± 2	69 ± 2	51 ± 1
K_M^{AcAc} (mM)	0.11 ± 0.01	0.092 ± 0.008	0.067 ± 0.009
K_M^{NADH} (mM)	0.010 ± 0.002	0.008 ± 0.001	0.007 ± 0.001
k_{cat}/K_M^{AcAc} (M^{-1} s^{-1})	7.9 ± 0.9 × 10^5	7.5 ± 0.6 × 10^5	7.6 ± 1.1 × 10^5
k_{cat}/K_M^{NADH} (M^{-1} s^{-1})	9.1 ± 1.4 × 10^6	9.1 ± 1.4 × 10^6	7.8 ± 1.3 × 10^6

[a]Values represent mean ± fitting error of duplicate measurements.

Table S9. Solvent viscosity effects on *Ab*HBDH steady-state kinetic parameters for 3-oxovalerate reduction at 298 K.[a]

Parameter	0% glycerol (*v/v*)	18% glycerol (*v/v*)	27% glycerol (*v/v*)
k_{cat} (s^{-1})	0.60 ± 0.03	0.74 ± 0.02	0.77 ± 0.02
$K_M^{3\text{-}OV}$ (mM)	0.056 ± 0.003	0.036 ± 0.004	0.038 ± 0.002
K_M^{NADH} (mM)	0.06 ± 0.01	0.028 ± 0.004	0.018 ± 0.003
$k_{cat}/K_M^{3\text{-}OV}$ (M^{-1} s^{-1})	1.1 ± 0.08 × 10^4	2.1 ± 0.2 × 10^4	2.0 ± 0.1 × 10^4
k_{cat}/K_M^{NADH} (M^{-1} s^{-1})	1.1 ± 0.2 × 10^4	2.6 ± 0.4 × 10^4	4.3 ± 0.7 × 10^4

[a]Values represent mean ± fitting error of duplicate measurements.

Table S10. Solvent viscosity effects on *Pa*HBDH steady-state kinetic parameters for 3-oxovalerate reduction at 298 K.[a]

Parameter	0% glycerol (*v/v*)	18% glycerol (*v/v*)	27% glycerol (*v/v*)
k_{cat} (s^{-1})	4.9 ± 0.1	3.94 ± 0.03	3.60 ± 0.06
$K_M^{3\text{-OV}}$ (mM)	0.036 ± 0.002	0.0274 ± 0.0004	0.034 ± 0.004
K_M^{NADH} (mM)	0.007 ± 0.002	0.0031 ± 0.0003	0.0032 ± 0.0003
$k_{cat}/K_M^{3\text{-OV}}$ (M^{-1} s^{-1})	1.4 ± 0.07 × 10^5	1.4 ± 0.02 × 10^5	1.1 ± 0.1 × 10^5
k_{cat}/K_M^{NADH} (M^{-1} s^{-1})	6.9 ± 0.2 × 10^5	1.3 ± 0.1 × 10^6	1.1 ± 0.1 × 10^6

[a]Values represent mean ± fitting error of duplicate measurements.

Table S11. *Pa*HBDH k_{STO} and k_{cat} for acetoacetate and 3-oxovalerate reduction.

	$k_{STO}^{40\mu M}$ (s^{-1})[a]	$k_{STO}^{50\mu M}$ (s^{-1})[a]	k_{cat} (s^{-1})[b]
Acetoacetate, 283 K	65.6 ± 0.3	66.7 ± 0.2	30 ± 1
3-Oxovalerate, 283 K	2.6 ± 0.1	2.9 ± 0.1	2.6 ± 0.2
3-Oxovalerate, 298 K	4.7 ± 0.1	5.4 ± 0.1	5.9 ± 0.1

[a]Values represent mean ± fitting error of at least 6 replicates.

[b]Values represent mean ± fitting error of at least duplicate measurements.

Table S12. *Ab*HBDH k_{STO} and k_{cat} for acetoacetate and 3-oxovalerate reduction.

	$k_{STO}^{40\mu M}$ (s^{-1})[a]	$k_{STO}^{60\mu M}$ (s^{-1})[a]	k_{cat} (s^{-1})[b]
Acetoacetate, 283 K	26.2 ± 0.1	27.4 ± 0.1	3.4 ± 0.1
3-Oxovalerate, 283 K	2.7 ± 0.1	3.1 ± 0.1	0.21 ± 0.01
3-Oxovalerate, 298 K	3.7 ± 0.1	4.4 ± 0.1	0.60 ± 0.03

[a]Values represent mean ± fitting error of at least 6 replicates.

[b]Values represent mean ± fitting error of at least duplicate measurements.

REFERENCES

1. Oke, M.; Carter, L. G.; Johnson, K. A.; Liu, H.; McMahon, S. A.; Yan, X.; Kerou, M.; Weikart, N. D.; Kadi, N.; Sheikh, M. A.; *et al*. The Scottish Structural Proteomics Facility: Targets, Methods and Outputs. *J. Struct. Funct. Genomics* 2010, *11* (2), 167–180.
2. Niesen, F. H.; Berglund, H.; Vedadi, M. The Use of Differential Scanning Fluorimetry to Detect Ligand Interactions That Promote Protein Stability. *Nat. Protoc.* 2007, *2* (9), 2212–2221.